Research of mechanical model based on characteristics of fracture mechanics of ice cutting for scientific drilling in polar region

Xinyu Lv[1, 3]**, Zhihao Cui**[2, 3]**, Ting Wang**[2]**, Yumin Wen**[2]**, An Liu**[4]**, Rusheng Wang**[2, 3*]

[1] Naval Architecture and Ocean Engineering College, Dalian Maritime University, Dalian 116026, China.

[2] College of Construction Engineering, Jilin University, Changchun, 130021, China

[3] Polar Research Center, Jilin University, Changchun, 130021, China

[4] Power China Huadong Engineering Corporation Limited, Hangzhou, 310014, China

Correspondence: Rusheng Wang (wangrs@ jlu.edu.cn)

Abstract:Scientific drilling in polar regions plays a crucial role in obtaining ice cores and using them to understand climate change and to study the dynamics of the polar ice sheet and its impact on global environmental changes (sea level, ocean current cycle, atmospheric circulation, etc.). Mechanical rotary cutting is a widely used drilling method that drives the cutter to rotate to cut and drill through ice layers. It is necessary to conduct in-depth research on the brittle fracture behavior of ice and mechanical model, and analyze the factors and specific mechanisms (cutter's angle, rotation speed of the drill bit, and cutting depth) affecting cutting force for the rational design of ice-core drill system, improving the efficiency of ice-core drilling, and ensuring the drilling process smoothly. Therefore, in this paper, the process of ice cutting was observed, the fracture mechanics characteristics of ice cutting process wad analyzed, the formation process of ice chips was divided into three stages, and the mathematical model for the cutting force was established based on the observation results. It describes the damage conditions of ice failure and points out the influencing factors and specific influencing laws on cutting force. Furthermore, the cutting force generated under various experimental conditions was tested. Based on typical real-time data curves of cutting force, the characteristics of cutting force were analyzed during the cutting and drilling process. Based on the comparison results of the average cutting force, the influence mechanism of various parameters on the cutting force is obtained. This proves the correctness of the mathematical model of the cutting force and provides a theoretical reference for the calculation of cutting force during ice cutting and drilling in polar regions.

1. Introduction

As the largest cold source on Earth, Polar ice sheets/glaciers are an important component of the Earth's system related to the Earth's crust, glaciers, ice shelf, ocean, and atmosphere, it has a profound impact on global changes such as climate change and sea level rise et al (Lin Yang et al., 2023). Many scientific issues related to polar regions can be solved and validated by carrying out scientific drilling in ice sheets and obtaining ice cores (S.H. Faria et al., 2014; P. Talalay et al., 2015; P.L. Cao et al l., 2019). Mechanical rotary drills have been widely used in the field of polar ice core drilling (Ueda and Garfield, 1968, 1969; Gundestrup et al., 1984; Kudryashov et al., 1994; Stanford, 1992; Wumkes, 1994; Shturmakov et al., 2007). The process of ice core drilling mainly consists of three steps: Cutting and drilling of the ice sheet, removal and transport of the ice chips generated at the hole bottom, and the collection of ice core and chips precipitation (Litvinenko VS and Nikolay I Vasiliev et al., 2014). These three steps are interrelated, and all of them have significant effects on the process of drilling. The cutting and drilling of the ice sheet generate a cutting force, which not only affects the selection of the motor system of the drill but also the design of the anti-torsion system, and even determines the success or failure of the cutting and drilling of the ice sheet. By conducting in-depth research on the fracture mechanics characteristics of solid ice, establishing a mechanical model for ice cutting, and determining the factors and specific mechanisms affecting cutting force, it can contribute to the rational design of the drilling tool system, the improvement of drilling efficiency, and ensure the smooth progress of drilling.

During ice core drilling, ice cutting is periodically carried out. At first, the moving cutters cut into the ice and compress it. When the level of stress near the edge of the cutter exceeds the cutting point, a crack is formed in the direction from the edge to the surface. This means that the horizontal force of cutting, called P_x, creates a repeated series of breaks, and its value is considered to be the mean force over the cutting length. Griffith (1920) assumed that when the energy of elastic strain exceeds the surface energy, the existing micro-crack starts to extend like an avalanche, and the materials break. Mellor and Sellman (1976) suggested that cutting force P_x can be calculated by using specific energy E_S (N/m^2), which is the energy consumed per unit of cutting volume:

$$P_x = bhE_S \tag{1}$$

where b is the width of the cutter; h is the depth of cut.

58   Using the formula (1) to calculate cutting force is difficult because specific energy is a vague

59   concept. The formula ignores the influence of the structure of the cutter on the cutting force and lacks a

60   certain degree of practicality. Due to the difficulty of conducting strict theoretical methods for the

61   design of rock-cutting machines, many of the same experimental methods were developed by Mellor

62   (1981). Maeno (1988) assumed that in any deformation process caused by compression, tension,

63   bending, or cutting, the mechanics of ice failure are determined by the processes of inter/intragrain

64   sliding. Taking the ideal monocrystal of ice, the theoretical stress needed for the formation of sliding

65   zones is near 100 MPa, but for real ice, it does not exceed 0.1– 0.5 MPa (Lavrov, 1969). The

66   contradiction is explained by the disposition theory. According to this theory, the deformation of the

67   ice is determined by the defects which already exist in the ice crystal. The internal defects gradually

68   expand under the action of external forces, the ice destruction occurs. Due to the non-uniformity, hard

69   brittle, and the factors that affect cutting resistance are complex, most studies on solid ice are

70   conducted to investigate the influence of a certain variable on cutting resistance (Chiaia, 2008; S. Hell

71   et al., 2014; A. Chao Correas et al., 2022). The in-depth study of the cutting properties of solid ice was

72   rarely reported.

73   In this paper, images of the cutting and drilling process of the ice under various experimental

74   conditions were captured, the fracture mechanics characteristics of the ice cutting process were

75   analyzed, and the formation process of ice chips was clear and divided into three stages. Based on the

76   result, a mechanics and mathematical model of ice cutting was built, and the influencing factors and

77   specific influencing laws on cutting force were analyzed. Finally, the influencing factors and laws were

78   verified through experimental tests. Which provides a theoretical reference for the calculation of

79   cutting force during ice cutting and drilling.

80   **2. Observation of ice fissure propagation in the process of ice cutting for ice-core drilling**

81   **2.1. Test stand design for study on ice cutting process**

82   To observe the cutting and drilling process of the ice under various experimental conditions, an ice

83   cutting and drilling simulation test stand has been designed (Fig. 1).
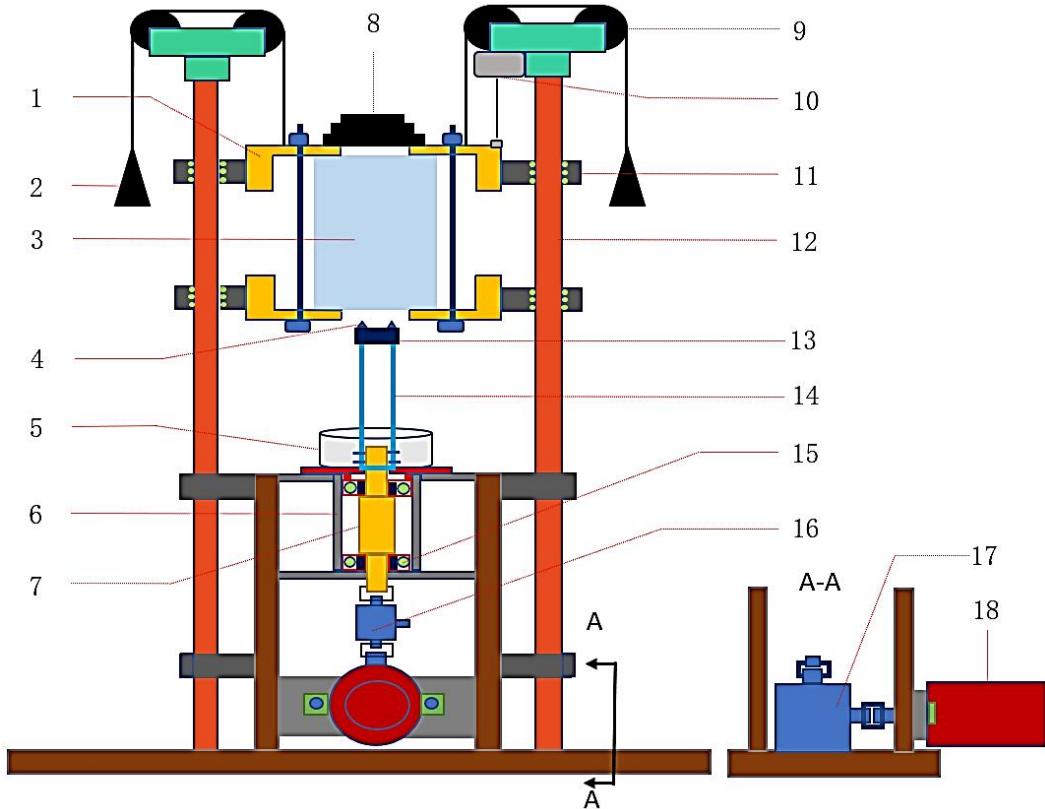
84

85 **Figure 1.** Schematic diagram of the experimental platform: 1-ice box; 2-balance weight 1; 3-ice block; 4-cutter;

86 5-ice chips collector; 6-cup set; 7-stepped shaft; 8-dead weight; 9-fixed pulley; 10-draw-wire displacement sensor;

87 11-slider; 12- slide rail; 13-drill bit; 14- drill pipe; 15- bearing; 16-torque sensor; 17- directional converter;

88 18-servo motor

89 To ensure the ice cutting and drilling proceed smoothly and the WOB is constant during the drilling

90 process, the drilling direction is inverted upward. Therefore, the ice chips generated in the drilling

91 process directly fall into the ice chips collector due to gravity, there will be no adhesion or blockage on

92 the drill bit. During the experimental process, the ice block and ice box can slide nearly frictionless as

93 they are connected to two parallel slide rails through four sliders, and the slider is equipped with rolling

94 balls inside to ensure that the slider slides almost frictionless on the slide rail. So, during the drilling

95 process, constant drilling pressure can be ensured, and multiple drilling pressure tests can be achieved

96 by increasing or decreasing balance weight and dead weight. The drill pipe, drill bit, and cutters are

97 driven to rotate by the servo motor system, and its rotation speed can be adjusted arbitrarily between

98 0-1000rpm. In this way, the adjustment of the rotation speed of the drill bit is achieved. The cutter

99 equipped in the experimental test stand can be replaced arbitrarily according to the experimental

100 requirements, therefore, it is possible to conduct cutting and drilling tests on cutters with various

101 structures.

102 During the experiment, the torque generated by driving the rotation of drill pipes, step shafts, and

103 other components, as well as the cutting torque generated by ice cutting is measured by the torque

104 sensor. Before conducting the cutting and drilling experiment, adjust the rotation speed of the drill bit

105 to the rotation speed for the next experiment, and let the drill bit and other components blank run. After

106 the torque measured by the torque sensor stabilizes, the torque is recorded as T_1. Next, perform cutting

107 and drilling. After the cutting and drilling process stabilizes, the recording of cutting torque begins.

108 after the drilling process, the average cutting torque during this period is recorded as T_2. So, the torque

109 for ice blocks cutting T_c can be calculated according to the following formula (2).

110
$$T_c = T_2 - T_1 \qquad(2)$$

111 The drilling depth and time are measured by the Draw-wire displacement sensor. The formation

112 process of ice chips is captured by a high-speed camera.

113 **2.2. Test stand building and observation of ice fissure propagation during ice-core drilling testing**

114 Based on the above working principle, the ice core drilling test stand has been established (Fig. 2)**.**

115
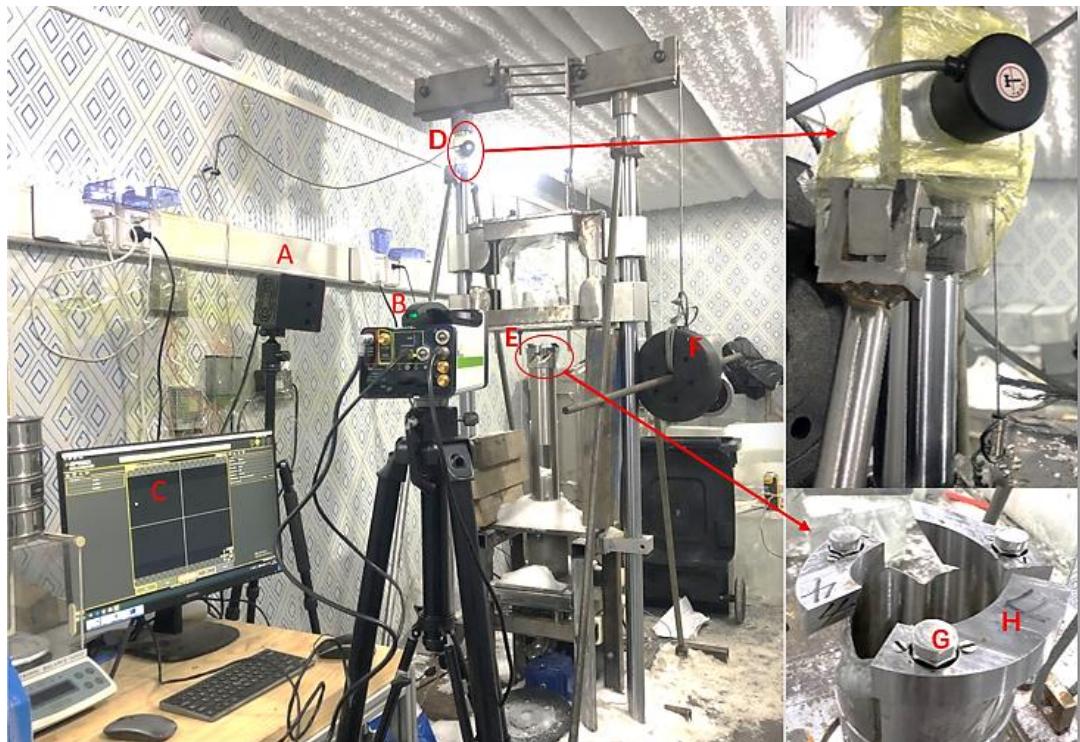
Figure 2. Test stand: A-light source; B-high speed camera; C-image display computer; D-draw-wire displacement sensor; E-drill bit; F-counterweight block; G-drill bit shoe; H-cutter

The specific parameters of the main equipment in the test stand are shown in Table 1.

Table 1. Main parameters of equipment

equipment and sensor		Model	Main parameters
Servo motor system	Driver	3DM2080-DSP	Drive voltage: 130-220VAC
			Pulse mode: Mono pulse
			Adjustment range: 0-1000rpm
	Motor	130BYG350D	Maximum output torque: 60N.M
			Step angle: 1.2°
			Rated voltage and current: 220V and 8.5A
	Pulse generator	CS10-3	Output mode: Steering + pulse
			Adjustment range: 0-1000rpm
			Output signal voltage: 5V; Power range:9-30V
Torque sensor		LLBLS-I	Measuring range: 60N.M: Overall accuracy:0.3%
			Maximum speed: 6000rpm
Draw-wire displacement sensor		MPS-M	Measuring distance:0-1500mm
			Resolving power:0.01mm;
			Pulling force of stay wire:4N
Slide rail and slider system		Ø50; SK50	Friction coefficient: 0.0010-0.0015
High-speed camera		Ispeed-7	Technology: CMOS active pixel
			Resolution: 2048×1536
			Frames per second: 1000000fps
			Shutter: 1us
			Lens options: F mount/G mount/C mount

Before the experiment, the cutters (Fig.2.H) made from tool steel (W18Cr4V) shall be installed on the drill bit (Fig.2.E) through bolts and pins (Fig.2.H) that also serve as the shoes with adjustable height. The height of the bolts is lower than the height of the cutter's tip when the ice block slides into contact with the shoes, the cutters have been cut into the ice block at the designed depth. Thus, the cutting and drilling at the designed cutting depth is realized and the cutting depth has been accurately controlled.

Aiming the high-speed camera (Fig.2.B) at the cutting edge of the cutter, adjusting the frame number of the high-speed camera to 100,000, meanwhile, supplementing the light on the object with the light source (Fig.2.A), until the image displayed in the computer (Fig.2.C) is clear. After the experiment, the images of the formation process of ice chips are captured and saved in a high-speed camera. The observation experiment of the cutting and drilling process is conducted under various experimental

130 conditions (multiple cutter angles, cutting depths, and rotation speed of drill bit). The specific

131 parameters of experimental conditions are shown in Table 2. The cutter used in the experimental

132 process are processed with wire cut technology. Before the experimental, to prevent the impact of

133 surface burrs, slag, and surface roughness on the test results, sandpapers with 1000 mesh, 1500 mesh,

134 and 2000 mesh ware selected respectively to manually polish the surface of the cutter until it was

135 smooth. After each test, the surface and cutting edge of the cutter are observed, if there is wear or

136 damage, the cutter is polished or replaced directly. The cutters- tested in the experiment are shown in

137 Fig. 3.

138

Table 2. The specific parameters of experimental conditions

| Width (mm) | Structure of cutter | | Cutting depth (mm) | Rotation speed (rpm) | Ice sample dimension (mm) | Ice core diameter (mm) |
	Rake angle (°)	Relief angle (°)				
25	20	5	1	50	~250×250×450	60
	30	10	2	100		
	40	15	3	150		

139

140 **Figure 3.** Multi-group structure cutters

141 This study mainly focuses on the establishment of mechanical model during the ice cutting and

142 drilling process. And, studies have shown that the crystal orientation, the crystal size and the density of

143 ice samples in NGRIP boreholes in Greenland are similar to naturally formed and artificially frozen ice

144 samples (Center for Ice and Climate, 2023). Moreover, many scholars have conducted experiments on

145 artificially prepared or naturally formed ice samples, and have ultimately obtained convincing

146 experimental data and conclusions, providing valuable references for research in the polar field

147 (Talalay, 2003; Hong et al.,2015; Wang et al, 2024). In order to better observe the formation process of

148 ice chip, at present stage, this study selected transparent ice and explored the fracture process and

149 cutting force generated by this type of ice. The ice with variety properties belongs to brittle materials,

150 and there will be similarities in the fracture process. In the future, the cutting and drilling experiments

151 with different ice sample properties to explores the effect of ice properties against the cutting force will

152 be carried out. The ice blocks used in this experiment are frozen by an ice-making machine (Fig.4),

153 which can produce transparent ice samples without bubbles. Then, we divided these blocks into

154 experimental ice blocks with uniform dimensions (Fig.5) of ~$250 \times 250 \times 450$ mm. and all tests were

155 carried out in the refrigerated container with a constant temperature of -15℃.

157 **Figure 4.** Ice-making machine   **Figure 5.** Experimental ice samples

158 **3. Analysis of characteristics of ice fracture mechanics in the process of ice cutting**

159 It is preliminary observed after the mechanical testing of ice under the special experimental

160 condition. The actual ice-cutting process captured by a high-speed camera is shown in Fig. 6.
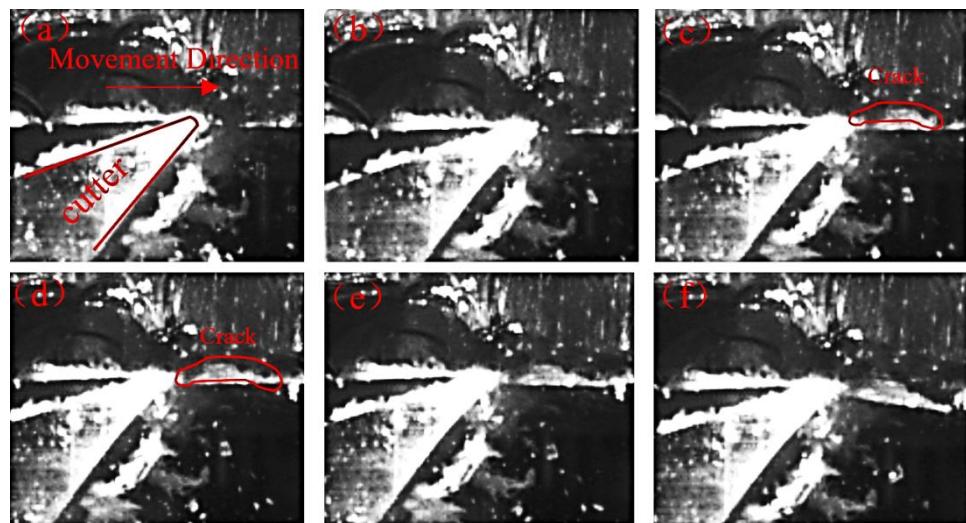
A (rake angle is 40°, relief angle is 15°, cutting depth is 1 mm and the rotation speed of the drill bit is
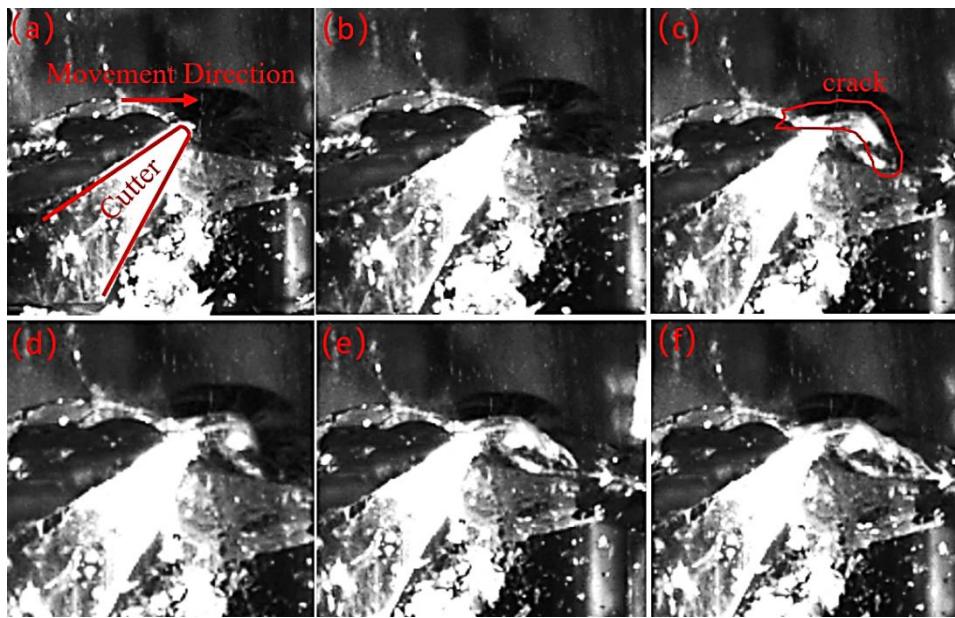
100 rpm)

B (rake angle is 30°, relief angle is 25°, cutting depth is 2 mm and the rotation speed of the drill bit is

100 rpm)

Figure 6. Cutting process captured by high-speed video camera

Compared with the cutting and drilling process at a cutting depth of 1mm, when cutting and drilling at a cutting depth of 2mm, the depth of the cutter inserted into the ice sample increases resulting in more small particle ice chips.The particle size of the ice chips formed by major fracture increases, and the surface after cutting becomes more uneven.

Under various experimental conditions, the ice cutting process is similar. In the cutting process, the cutting of the ice is constantly repeated, the main damaged form of ice is a brittle fracture, the chips show wedge block with no significantly deform, and wedge-shaped ice chips with different particle sizes are constantly formed under variety experimental conditions. The formation process of a single large particle of ice chips can be divided into three stages. In the first stage, the cutter invades the ice, and the ice is compressed by the rake and relief surfaces of the cutter, resulting in ice crushing and smaller ice chip formation (Fig. 6. a, b). In the second stage, with the rotation of the drill bit, cracks appeared in the ice, and the cracks began to expand along a direction that approximately presented an angle of 45° with the horizontal direction (Fig. 6. c, d). However, there were no gaps or separations between the ice and cutters on both sides of the cracks. In the third stage, the cutter moved forward, the

182   crack expanded to form ice chips with large particle size that slid forward, and finally detached from

183   the ice. At the same time, ice chips with small particle sizes were also generated on the sliding surface

184   (Fig. 6. e, f).

4. Study on a mechanical model of ice cutting process

4.1. Mechanical model building based on the characteristics of ice fracture mechanics

187   According to the observation results of the ice cutting, it can be considered that the damage of the ice

188   is the result of shear slip failure caused by the compression effect of the cutter. In this process, the force

189   exerted on the ice chips mainly includes the squeezing force F_n towards the ice, and along the normal

190   direction of the cutter's rake face. The frictional force F_m exerted by the cutter when the ice chips

191   flow out; At the same time, the shear surface of the ice will also be subjected to normal pressure F_{ns}

192   and shear force F_s. Before the cutting of the ice, these two pairs of forces are in equilibrium. The

193   relationships between these forces are analyzed in front of the cutting edge (Fig. 7).
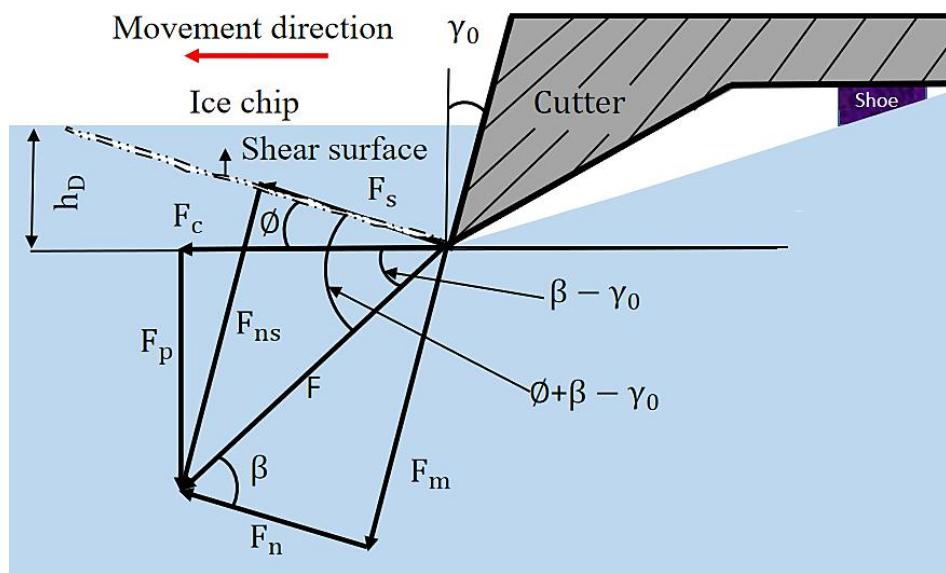
194

195   **Figure 7.** Relationship between force and angle

196   Where F is the combined force of F_m and F_n, $\emptyset$ is the shear angle, β (Friction angle) is the angle

197   between F_n and F, γ_0 is the rake angle of the cutter, F_p is the component force perpendicular to the

198   movement direction of the cutter, which is applied to the cutter and mainly provided by the weight on

199   drill bit during the ice layer cutting and drilling, causing the cutter to cut into the ice to a certain depth.

200   During the cutting and drilling process, the cutter comes into contact with the ice sample before the

201   shoes. Only when the cutter is inserted into the ice layer with designed cutting depth, the shoes will

202   fully contact the bottom of the borehole. Prior to this, there will be continuous F_p on the cutter. As the

203   drill bit rotates, the cutter always inserts the ice sample before the shoe, and the F_p on the cutter will

204   continue to exist. Where F_c is the component force acting on the ice layer, and during the ice layer

205   cutting and drilling process, this force is mainly provided by the motor, which is called the cutting

206   force. h_D is the cutting thickness. If the cutting width is represented by b_D, The cutting width

207   represents the width of the annular gap between the ice core and the hole wall in the process of ice

208   drilling (cutting width, width of the cutter), The area of the nominal cross-section of the cutting layer is

209   represented by A_D ($A_D = h_D b_D$), The area of shear surface is represented by A_s ($A_s = A_D/sin\emptyset$), the

210   shear stress on the shear plane is represented by τ, then

211
$$F_s = \tau A_s = \frac{\tau A_D}{sin\emptyset} \qquad (3)$$

212   According to Fig. 7, it can be concluded that:
213
$$F_s = Fcos(\emptyset + \beta - \gamma_0) \qquad (4)$$
214   According to the relationship between various forces, it can be concluded that:

215
$$F = \frac{F_s}{cos(\emptyset+\beta-\gamma_0)} = \frac{\tau A_D}{sin\emptyset cos(\emptyset+\beta-\gamma_0)} \qquad (5)$$

216
$$F_p = Fsin(\beta - \gamma_0) = \frac{\tau A_D sin(\beta-\gamma_0)}{sin\emptyset cos(\emptyset+\beta-\gamma_0)} \qquad (6)$$

217
$$F_c = Fcos(\beta - \gamma_0) = \frac{\tau A_D cos(\beta-\gamma_0)}{sin\emptyset cos(\emptyset+\beta-\gamma_0)} \qquad (7)$$

218   **4.2. Analysis of factors influencing cutting forces via the mechanical model**

219   According to Fig. 7, there is no shear stress in the plane perpendicular to the combined force F, so

220   the main stress is completely determined by the F. The material is in the state of plane stress, and the

221   included angle between the direction of the maximum shear stress and the direction of the maximum

222   principal stress is 45°, the included angle between the maximum principal stress and the F is 45 °, then

223   there is:

224
$$\emptyset + \beta - \gamma_0 = \frac{\pi}{4} \qquad (8)$$

225   So:

226
$$\emptyset = \frac{\pi}{4} - \beta + \gamma_0 \qquad (9)$$

227   The shear angle $\emptyset$ is affected by the rake angle of the cutter γ_0 and friction angle β. As the rake

228   angle of the cutter γ_0 increases, the shear angle $\emptyset$ increases; as the friction angle β increases, $\emptyset$

229   decreases.

230   The area of the nominal cross-section of the cutting layer is represented by A_D $(A_D = h_D b_D)$, The

231   area of the shear surface is represented by A_s $(A_s = A_D/sin\emptyset)$, the shear stress on the shear plane is

232   represented by τ, then, according to equation (5) and the relationship between the nominal

233   cross-section and the shear plane, it can be obtained that:

234
$$F_c = \frac{\tau A_D \cos(\beta - \gamma_0)}{sin\emptyset \cos(\emptyset + \beta - \gamma_0)} \qquad (10)$$

235   When the ice is about to break, the shear stress on the shear plane reaches its maximum value. This

236   value is determined by the properties of the ice and will not change as the drilling conditions. Therefore,

237   the cutting force is influenced by the cutting width of the cutter and the cutting depth. The cutting force

238   shows a linear increasing trend with the increase of the cutting width and the cutting depth. In addition,

239   the cutting force is also affected by the shear angle $\emptyset$、friction angle β, and cutter's rake angle γ_0. The

240   friction angle β is a certain value as the properties of the ice and cutter's material. The shear angle $\emptyset$ is

241   determined by the friction angle and the cutter's rake angle as shown in formula (9). Substituting

242   equation (9) into (10) and solving for the combined cutting force F_c, the following equation can be

243   given:

244
$$F_c = \frac{\tau h_D b_D \cos(\beta - \gamma_0)}{\sin\left(\frac{\pi}{4} - \beta + \gamma_0\right)\cos\left(\frac{\pi}{4}\right)} \qquad (11)$$

245   After simplifying the above equation, it can be obtained that:

246
$$F_c = \frac{2\tau h_D b_D}{1 - \tan(\beta - \gamma_0)} \qquad (12)$$

247   It can be seen from the formula (12) that the factors affecting the cutting force mainly consist of four

248   sides: The first aspect, it related to the shear strength of the ice, with the increase of shear strength, the

249   cutting force increases gradually. The second aspect, it influenced by the cutting depth, with the

250   increase of cutting depth, the cutting force increases gradually. The third aspect, it affected by the

251   cutting width, with the increase of cutting width, the cutting force increases gradually. Finally, the rake

252   angle of the cutter also has an impact on the cutting force. Formula (12) shows that: within the $\beta -$

253   $\gamma_0 \leq \frac{\pi}{2}$ range, as the rake angle of the cutter γ_0 increases, $\beta - \gamma_0$ gradually decreases, and the

254   $\tan(\beta - \gamma_0)$ decreases, $1 - \tan(\beta - \gamma_0)$ increases, F_c decreases.

255   **5. Test on the characteristics of cutting force and its influencing factors for verifying the**

256   **mechanical model**

257 **5.1 Analysis of the characteristics of cutting force**

258 To verify the theoretical analysis results of the factors affecting cutting force, the cutting torque

259 collected by the torque sensor under various cutter angles, rotation speed of the drill bit, and cutting

260 depth conditions were measured.

261 After the experiment, the torque for ice cutting and drilling can be obtained through formula (2). The

262 schematic diagram of the torque and cutting force generated during the ice cutting drilling process is

263 shown in Figure 8, The relationship between the cutting force F_c generated by cutting the area of the

264 circular ring and the torque T_c measured by the torque sensor is as follow.

265               $$T_c = F_c r_A \tag{13}$$

266 Where r_A is the average radius of the circular ring.
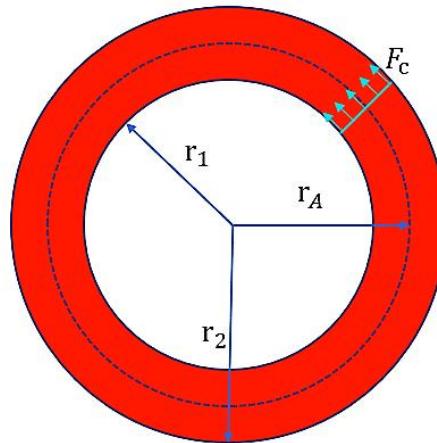
267

268 **Figure 8.** The schematic diagram of the torque and cutting force

269 By processing the data collected by the torque sensor, the cutting force generated by one cutter

270 during the ice block cutting and drilling is obtained. The typical cutting force trace generated during the

271 ice cutting process is shown in Fig. 9.
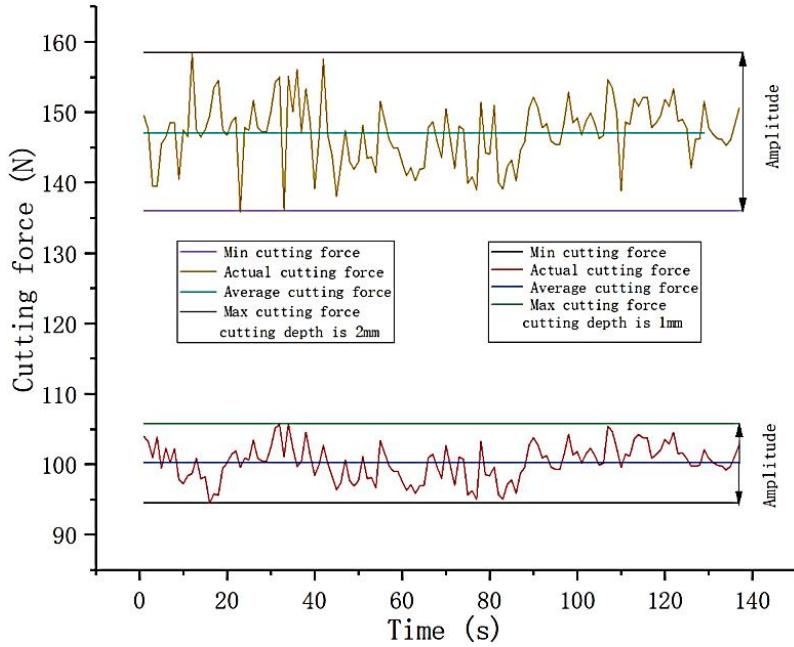
Figure 9. Typical cutting force trace(Cutting depth is 1 mm and 2 mm; Rotation speed of drill bit is 50rpm; Rake angle is 30°; Relief angle is 5°)

Fig. 9 shows the cutting force trace generated during two cutting and drilling process, which were carried out under the same conditions except for cutting depth, both cutting force traces oscillate at a certain frequency within a certain range, and the oscillation consists primarily of two frequencies, in addition the oscillation frequencies of two cutting force trace are similar. The higher frequency is related to the resolution of the sensor. The sensor outputs data at a certain interval during the recording process, the output data is not continuous, resulting in fluctuations in the trace. The lower frequency is related to the formation of large particle ice chips. Unlike ductile materials, where the chips produced by a shearing action are continuous and the forces appeared relatively constant, chips from brittle materials are produced by a repeated series of breaks. When the cutter is pressed into the ice, the cutting force begins to rise and elastic energy is stored in the cutter assembly, some of the energy is expended in local crushing, the ice layer undergoes shear-slip deformation. As the cutting force reaches a magnitude necessary to induce a major fracture, a crack propagates into the ice, releasing the cutter elastic energy and dislodging a major chip, the force than suddenly decreases. Therefore, during the cutting and drilling process in the ice layer, the cutting force trace exhibits an oscillating state, the amplitude of the oscillation is related to the cutting depth. During the process of the cutting depth increase, the degree of rapid increase and decrease in cutting force will be more severe. As show in Fig.

291 9, when drilling with a cutting depth of 2 mm, the oscillation amplitude of cutting force is greater than

292 that of drilling with a cutting depth of 1 mm.

293   As the cutting depth increases, the degree of crack propagation into the ice will also increase. When

294 the crack extends into the ice core, it will cause a decrease in the surface quality of the ice core. It is

295 necessary to control the cutting depth reasonably during the cutting process to ensure the quality of the

296 ice core. Moreover, the study results on mechanical models of ice cutting process indicated that:

297 "within the range of $\beta - \gamma_0 \leq \frac{\pi}{2}$, the cutting force gradually decreases with the increase of the rake

298 angle". The rake angle can be appropriately increases within this range to reduce the oscillation.

299 **5.2. Test of the factors influencing cutting force**

300   After the cutting and drilling experiments, the average cutting force was obtained under each

301 experimental condition. Plots of the average cutting force versus the cutter's rake angle are shown in

302 Fig. 10.
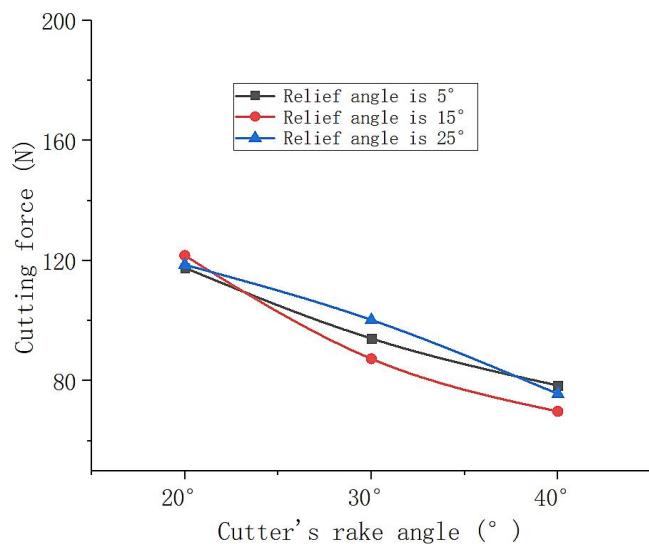
303

304   (a) The cutting depth is 1 mm, and the rotation speed of the drill bit is 100rpm
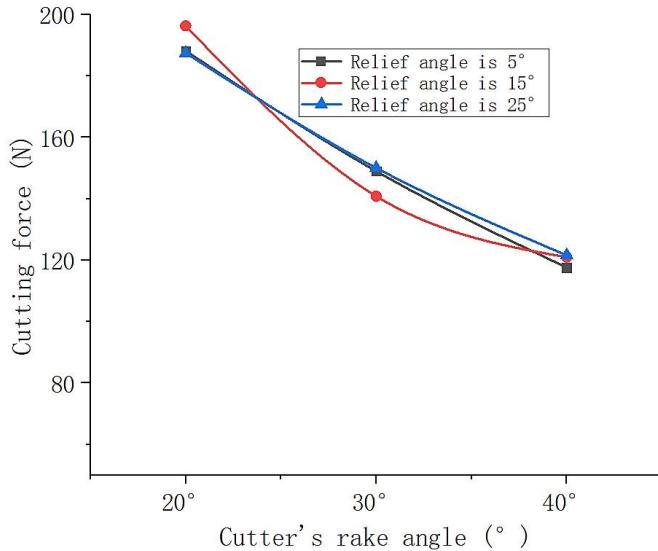
305

306   (b) The cutting depth is 2 mm, and the rotation speed of the drill bit is 100rpm
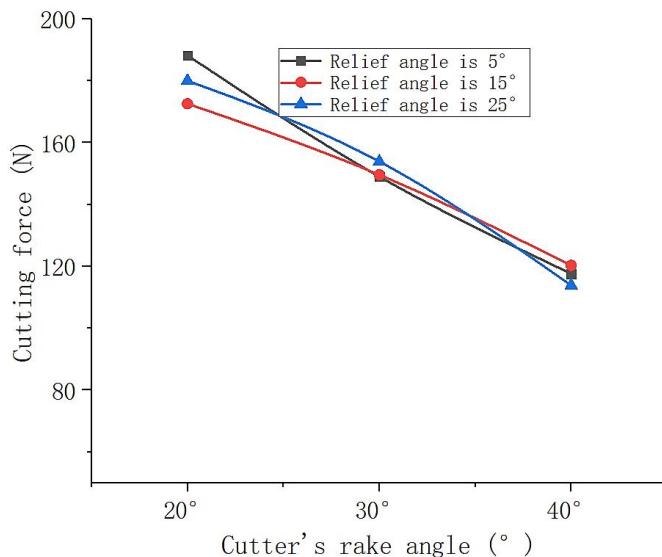
307

308   (c) The cutting depth is 2 mm, and the rotation speed of the drill bit is 50rpm

309   **Figure 10.** Cutting force versus cutter's rake angle

310   As shown in Fig. 10, when the cutting depth is 2mm, the rotation speed of the drill bit is 100 rpm,

311   and the rake angle of the cutter is 20 °, the cutting force reaches the maximum value of 196.3451N.

312   When the cutting depth is 1mm, the rotation speed of the drill bit is 100 rpm, and the rake angle of the

313   cutter is 40 °, the cutting force reaches the minimum value of 69.83529N. The cutting force varies

314   within this range under the other experimental conditions. That is, under various cutting depths and

315   drill speed conditions, the cutting force gradually decreases with the increase of the cutter's rake angle.

316   Plots of the average cutting force versus the cutter's relief angle are shown in Fig. 11.
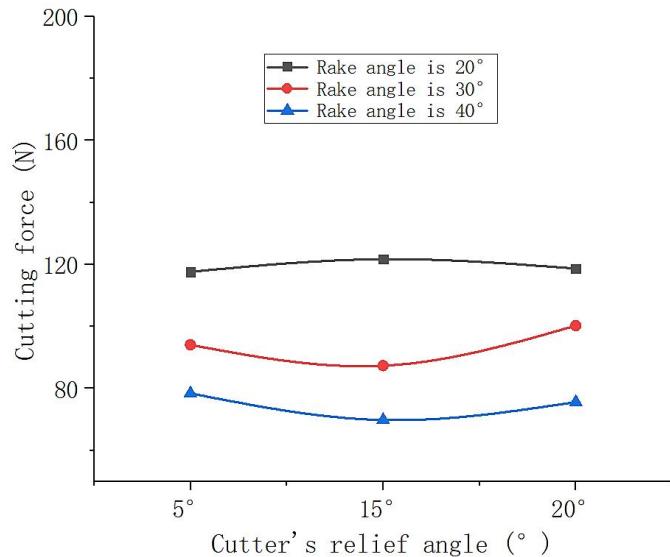
317

(a) The cutting depth is 1 mm, and the rotation speed of the drill bit is 100rpm

318
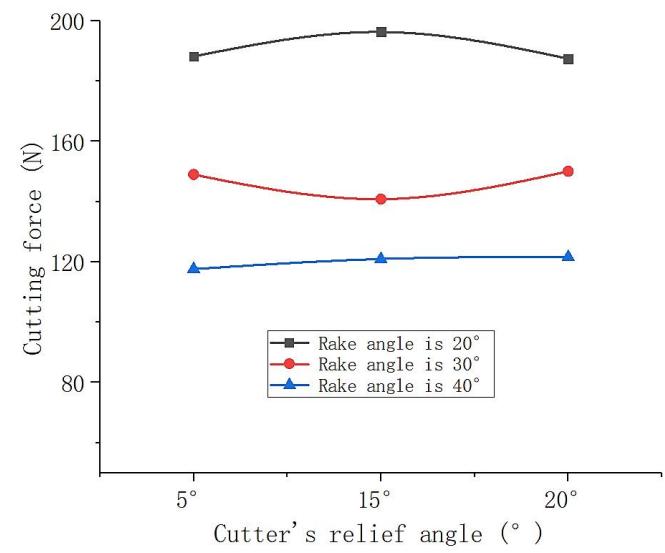
319

320

(b) The cutting depth is 2 mm, and the rotation speed of the drill bit is 100rpm
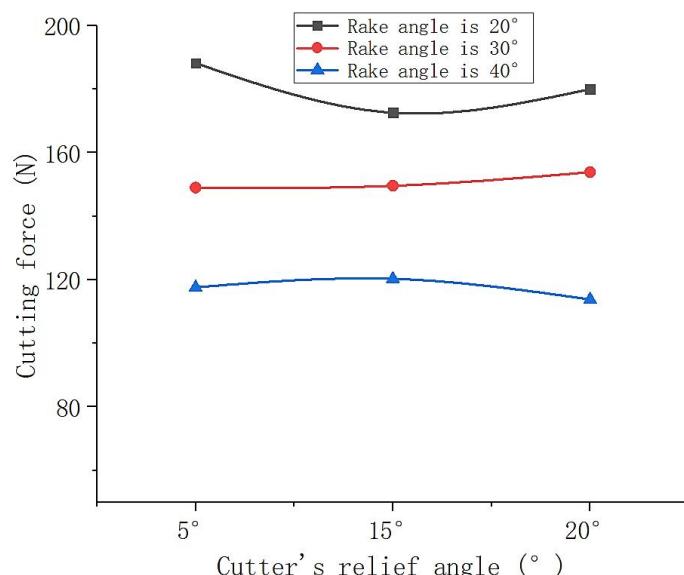
321

323   **Figure 11.** Cutting force versus cutter's relief angle

324    Under various experimental conditions, the relief angle of the cutter changes, and the cutting force

325  only changes slightly. Moreover, with the change of the relief angle of the cutter, the cutting force does

326  not show a clear and consistent change pattern. Therefore, it can be inferred that the relief angle of the

327  cutter has no clear effect on the cutting force.

328    Plots of the average cutting force versus the rotation speed of the drill bit are shown in Fig. 12.

329
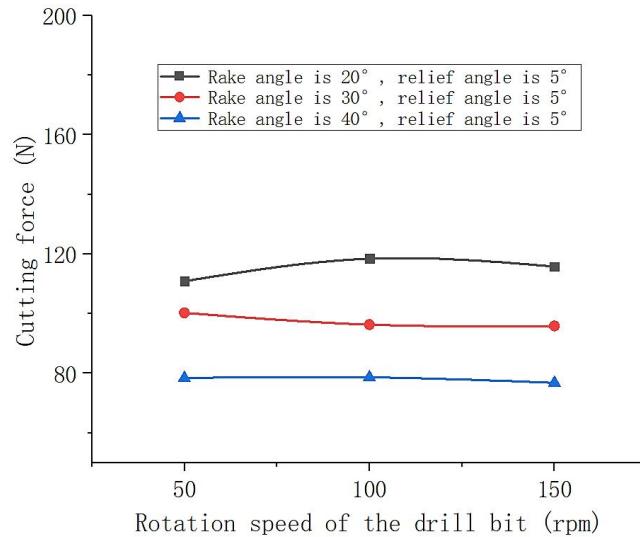
330            (a) The cutting depth is 1mm

331
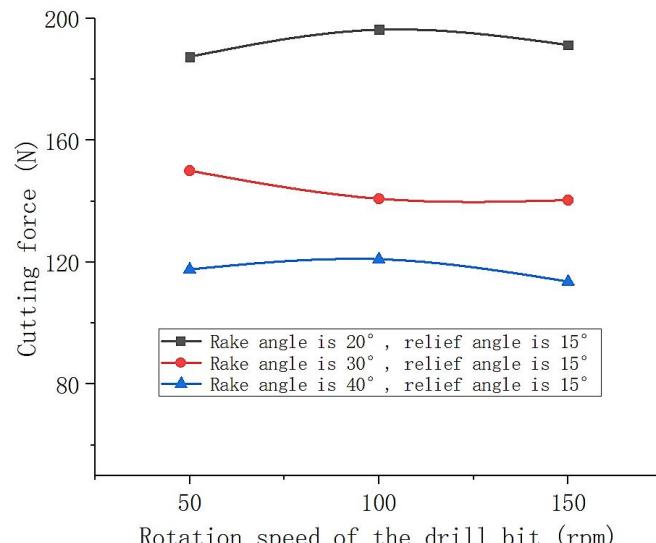
332           (b) The cutting depth is 2mm
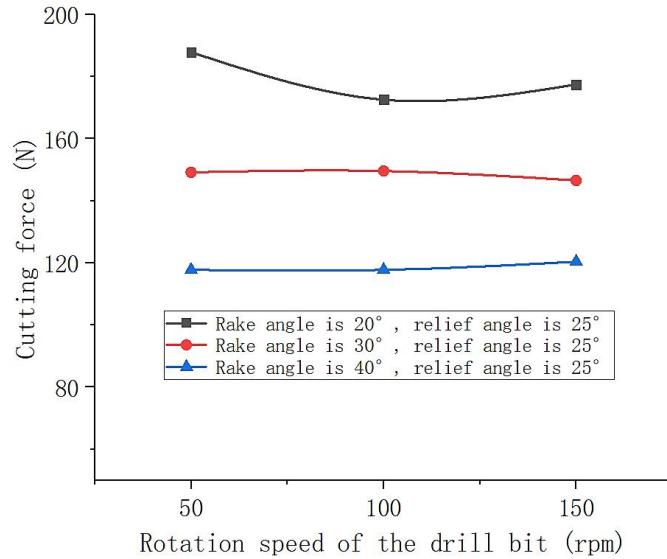
333

334 (c) The cutting depth is 2mm

335 **Figure 12.** Cutting force versus rotation speed of the drill bit

336   Under various experimental conditions, there is only a slight change in cutting force during the process of the

337 rotation speed changing, and there is no clear pattern of change. The rotation speed of the drill bit does not affect

338 the cutting force.

339   Plots of the average cutting force versus cutting depth are shown in Fig. 13.
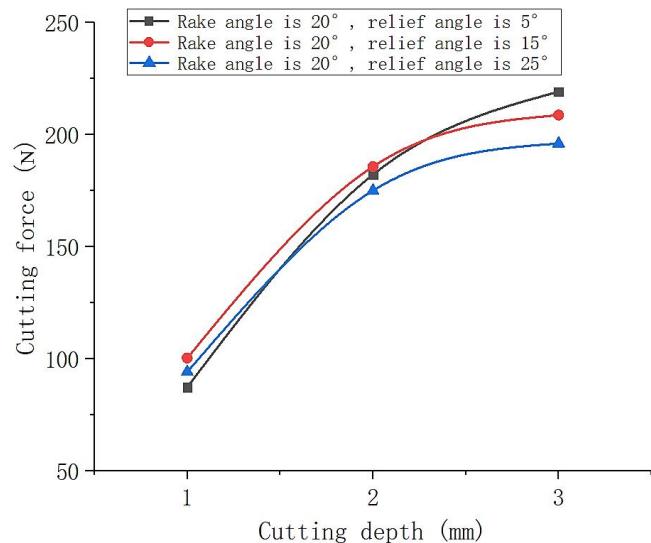
340

341 (a) The rotation speed of the drill bit is 50 rpm

342
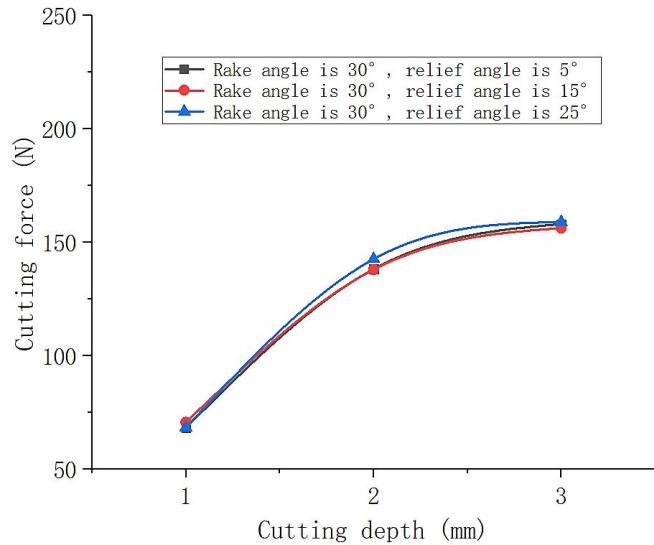
343 (b) The rotation speed of the drill bit is 100 rpm

344

345
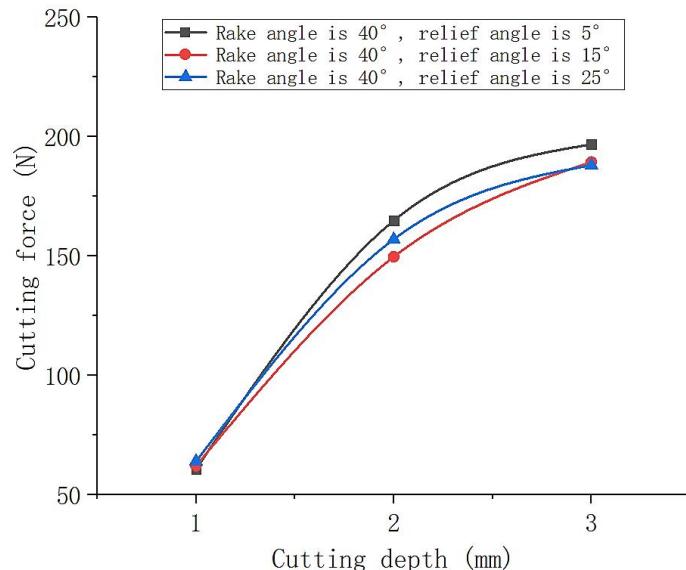
346 (c) The rotation speed of the drill bit is 100 rpm

347 **Figure 13.** Cutting force versus cutting depth

348   Under all experimental conditions, as the cutting depth increases, the cutting force shows a gradually

349 increasing trend. When the cutting depth is 3mm, the maximum cutting force reaches 219.13725N. And,

350 under the same experimental condition, the cutting depth increasing from 1 mm to 2 mm results in an

351 approximate doubling of the cutting force. As the depth of penetration increases, the cutting force

352 continues to increase, but the increasing trend gradually weakens.

353 **6. Conclusions**

354   It is preliminarily observed after the mechanical testing of ice, that the main damage form of ice is a

355   brittle fracture in the cutting process. During this process, the cutters press into the ice to a certain

356   depth and rotate, the ice withstands a squeezing effect from the rake face of the cutter and the shear slip

357   deformation occurs. When the shear slip deformation reaches a certain degree, the ice undergoes shear

358   failure and then forms ice chips. This process is constantly repeated throughout the cutting and drilling

359   of the ice.

360   Based on the characteristics of ice cutting and the stress characteristics during the ice cutting and

361   drilling process, a mechanical model of ice cutting was established. The mechanical model shows that

362   the cutting force is not only affected by the mechanical properties of ice but also by the cutting width,

363   cutting depth, and the rake angle of the cutter. As the cutting width and cutting depth increase, the

364   cutting force increases; as the increase of rake angle of the cutter, the cutting force decreases.

365   Additionally, the characteristics of cutting force were analyzed through experimental methods. The

366   experimental results show that the cutting force traces oscillated within a certain range, the oscillation

367   consists primarily of two frequencies. The higher frequency is related to the resolution of the sensor,

368   the lower frequency is related to the formation of large particle ice chips. the oscillation amplitude of

369   the cutting force traces is related to the cutting depth, as the cutting depth increases, the oscillation

370   amplitude of the trajectory will also increase. In addition, the oscillation amplitude will also affect the

371   quality of the core, as the amplitude increases, the possibility of the ice core breaking will also increase,

372   and the quality of the ice core will also increase accordingly. It is necessary to control the cutting depth

373   reasonably during the cutting process to ensure the quality of the ice core. Finally, the influencing

374   factors and laws of cutting force were verified by analyzing the cutting force generated under various

375   experimental conditions.

376

377   *Date availability.* No data sets were used in this article

378

379   *Author contribution.* Xinyu Lv: Conceptualization, Methodology, Writing – original draft; Zhihao Cui:

380   Methodology, Validation, Formal analysis, Visualization; Ting Wang: Methodology, Validation,

381   Formal analysis, Visualization; Yumin Wen: Conceptualization, Writing – review & editing,

382 Methodology, Validation; An Liu: Methodology, Validation, Formal analysis, Visualization; Rusheng

383 Wang: Methodology, Formal analysis, Supervision, Project administration, Funding acquisition.

384

385 *Competing interests*. The contact author has declared that neither of the authors has any competing

386 interests.

387

388 *Disclaimer. Publisher's note:* Copernicus Publications remains neutral with regard to jurisdictional

389 claims in published maps and institutional affiliations.

390

391 *Special issue statement*. This article is part of the special issue "Ice core science at the three poles

392 (CP/TC inter-journal SI)". It is not associated with a conference.

393

394 *Financial support*. This paper presents research conducted with support from the National Key R&D

395 Program of China (Project No. 2021YFA0719100; Subject No. 2021YFA0719103), and Jilin

396 University "Interdisciplinary Integration and Innovation" project (Project No. 419021421601).

397

398 **References**

399 Lin Yang, Guangju Zhao, Xingmin Mu, Yanli Liu, Peng Tian, Puqiong, Danzengbandian, Historical
400 and projected evolutions of glaciers in response to climate change in High Mountain Asia,
401 Environmental Research, Volume 237, Part 2, 2023, 117037, ISSN 0013-9351.
402 https://doi.org/10.1016/j.envres.2023.117037.

403 S.H. Faria, I. Weikusat, N. Azuma, The microstructure of polar ice. Part I: Highlights from ice core
404 research[J], J. Struct. Geol. 61 (2014) 2–20.
405 https://doi. org/10.1016/j.jsg.2013.09.010.

406 P. Talalay, C. Yang, P. Cao, et al., Ice-core drilling problems and solutions[J], Cold Reg. Sci. Technol.
407 120 (2015) 1–20.
408 https://doi.org/10.1016/j.coldregions.2015.08.014.

409 P.L. Cao, H.Y. Cao, J.E. Cao, et al., Studies on pneumatic transport of ice cores in reverse circulation
410 air drilling[J], Powder Technol. 356 (2019) 50–59.
411 https://doi. org/10.1016/j.powtec.2019.08.001.

412 Herbert T Ueda , Donald E Garfield (1968) Driling Through the Greenland Ice sheet. CRREl Specia/
413 Report 126, 1-7.
414 http://hdl.handle.net/11681/11876

Herbert T Ueda , Donald E Garfield (1969) Core Driling Through the Antarctic Ice Sheet. CRREl
        Technical Report 231, 1-19
        http://hdl.handle.net/11681/5654
Niels S Gundestrup , Sigfús J Johnsen, Reeh N (1984) ISTUK: A deep ice core drill
        system. Proceedings of the Second International Workshop/Symposium on Ice Drilling
        Technology (eds G. Holdsworth, K.C. Kuivinen and J.H. Rand), CRREL Special Report 84-34 ,
        7-19 .
Kudryashov BB , Nikolay l Vasliev, Pavel Talalay (1994) KEMs-112 electromechanical ice core
        drill. Memoirs of National institute of Polar Research, specialissue 49.138-152 .
Kerry L stanford (1992) An Engineering, Environmental and Logistical Analysis of the Polar lce
        Coring Office 13.2 cm lce Coring systemPICO CP-92-02,2-13.
Mark A Wumkes (1994) Development of the U.S. deep coring ice drill. Memoirs of National
        Institute of Polar Research. Special issue 49 , 41-51 .
        https://ci.nii.ac.jp/naid/110000010310
Alexander J Shturmakov, Donald A Lebar, William P Mason, Charles R Bentley (2007) A new 122
        mm electromechanical drill for deep ice-sheet coring (DISC): 1. Design concepts. Annals of
        Glaciology, 47, 28-34. doi: 10.3189/172756407786857811.
        https://doi.org/10.3189/172756407786857811
Litvinenko VS, Nikolay I Vasiliev, Volodya Ya Lipenkov, Dmitriev AN, Podoliak AV (2014).
        Special aspects of ice drilling and results of 5G hole drilling at Vostok station,
        Antarctica. Annals of Glaciology, 55, 68, 173-178.
         https://doi: 10.3189/2014AoG68A040.
Mellor, M., Sellman, P.V., 1976. General consideration for drill system design. Ice-Core Drilling.
        Proc. of the Symp., Univ. of Nebraska, Lincoln, USA, 28–30 Aug. 1974. University of
        Nebraska Press, Lincoln, pp. 77–111.
Mellor, M., 1981. Mechanics of cutting and boring: Part 7. Dynam78 P.G. Talalay / Cold Regions
        Science and Technology 37 (2003) 69–79.
         https://doi:10.1016/S0890-6955(02)00276-6
Maeno, N., 1988. Nauka o l'de (Science About Ice). Mir, Moscow. Text in Russian, 231 pp.
Lavrov, V.V., 1969. Deformatsia i prochnost' l'da (Deformation and Strength of Ice).
        Gidrometeoizdat, Leningrad. Text in Russian, 208 pp.
Chiaia., 2008. Triggering of dry snow slab avalanches: stress versus fracture mechanical approach [J].
        Cold Regions Science and Technology,2008,53:170–178.
        https://doi:10.1016/j.coldregions.2007.08.003
S. Hell, P. Weißgraeber, J. Felger, W. Becker, A coupled stress and energy criterion for the
        assessment of crack initiation in single lap joints: A numerical approach, Engineering Fracture
        Mechanics, Volume 117, 2014, Pages 112-126, ISSN 0013-7944.
        https://doi.org/10.1016/j.engfracmech.2014.01.012.
A. Chao Correas, P. Cornetti, M. Corrado, A. Sapora, Dynamic crack initiation by Finite Fracture
        Mechanics, Procedia Structural Integrity, Volume 42, 2022, Pages 952-957, ISSN 2452-3216.
        https://doi.org/10.1016/j.prostr.2022.12.120

456   Center for Ice and Climate, 2023. Niels Bohr Institute, University of Copenhangen[EB/ OL].
457   http://www.iceandclimate.nbi.ku.dk/research/ffowoffce/ice_crystal_structure/
458   Talalay, Pavel, 2003. Power consumption of deep ice electromechanical drills. Cold Reg. Sci.
459   Technol. 37 (1), 69–79.
460   https://doi.org/10.1016/S0165-232X (03)00036-3.
461   Hong, J., et al., 2015. Size distribution and shape characteristics of ice cuttings produced by an
462   electromechanical auger drill. Cold Reg. Sci. Technol. 119, 204–210.
463   https://doi.org/10.1016/j.coldregions.2025.08.012
464   Rusheng Wang, Xinyu Lv, Xiaopeng Fan, Da Gong, An Liu, Key parameters and mechanisms of ice
465   cores autonomously breaking with air reverse-circulation drill systems, Cold Regions Science
466   and Technology, Volume 217, 2024, 104053, ISSN 0165-232X.
467   https://doi.org/10.1016/j.coldregions.2023.104053.